Ni-Centered Coordination-Induced Spin-State Switching Triggered by Electrical Stimulation

Shaymaa Al Shehimy, Orsola Baydoun, Sandrine Denis-Quanquin, Jean-Christophe Mulatier, Lhoussain Khrouz, Denis Frath, Élise Dumont, Muralee Murugesu, Floris Chevallier, Christophe Bucher

Ni-centered Coordination-Induced Spin-State Switching Triggered by Electrical Stimulations

Shaymaa Al Shehimy, Orsola Baydoun, Sandrine Denis-Quanquin, Jean-Christophe Mulatier, Lhoussain Khrouz, Denis Frath, Élise Dumont, Muralee Murugesu, Floris Chevallier,* and Christophe Bucher*

ENSL, CNRS, Laboratoire de Chimie UMR 5182, 46 allée d'Italie, 69342 Lyon, France

KEYWORDS: Metalloporphyrin, Nickel, π-Dimer, Spin Switch, Viologen

ABSTRACT: We herein report the synthesis and the magnetic properties of a Ni(II)-porphyrin tethered to an imidazole ligand through a flexible electron-responsive mechanical hinge. The latter is capable of undergoing a large amplitude and fully reversible folding motion under the effect of electrical stimulation. This redox-triggered movement is exploited to force the axial coordination of the appended imidazole ligand onto the square planar Ni(II) center, resulting in a change in its spin state from low spin (S = 0) to high-spin (S = 1) proceeding with an 80% switching efficiency. The driving force of this reversible folding motion is the π-dimerization between two electrogenerated viologen cation radicals. The folding motion and the associated spin state change are demonstrated on the grounds of NMR, (spectro)electrochemical and magnetic data supported by quantum calculations.

INTRODUCTION

Molecules exhibiting switchable magnetic properties have been extensively studied over the past few decades in the context of the miniaturization of electronics, sensors and memory devices.[1–9] This particular field of magnetic switching has been the subject of major developments fueled by numerous research activities focused on molecular spin crossover (SCO) materials[10–13] and single molecule magnets.[14–17] Most exemples described so far are crystalline solids obtained from first-row transition metal complexes (d^4 to d^7) capable of undergoing spin state transition as a response to external physical perturbations such as temperature, pressure and light.[1,12,18] From a practical point of view, SCO phenomena are quite often difficult to explain from well-defined molecular events, they are strongly dependent on cooperativity processes between spin carriers and remain mostly limited to solid samples of coordination polymers subjected to low temperatures.[13,19–22]

These limitations have led to the emergence of alternative concepts aiming at triggering the rearrangement of electrons in discrete metal complexes both at room temperature and in solution. It includes the Coordination-Induced Spin-State Switching (CISSS) approach[23–27] where spin state transitions, *e.g.* from a high spin (HS) to a low spin (LS) state, are triggered by rational/drastic modifications of the first coordination sphere of a given metal center upon stimulation. The few examples reported to date in the literature involve a quite limited number of transition metals, namely Fe(II)[27–29], Mn(V)[30] or Ni(II),[23,24,31–36] selected for their ability to undergo HS↔LS transitions following the addition or removal of ligand(s) from the metal center (Figure 1a).[31,37] All of these achievements involve the use of chemicals (pH)[27,38,39] or light[23,31–35,40,41] as triggers for molecular motions leading to an increase or decrease in the coordination number of the metal. In contrast, far less progress has been made in these directions with electron-responsive systems, even though electricity stands as a particularly attractive, controllable and clean trigger in the perspective of applications in solid-state devices. [42–44] The few examples of redox-triggered magnetic switching reported so far in literature are based on Prussian blue analogs or on transition metal complexes exhibiting valence tautomerism.[45–49]

In this work, we report the synthesis and magnetic properties of an electrically-triggered Coordination-Induced Spin-State Switch operating on the intramolecular self-locking principle depicted in Figure 1b.[50] The latter shows how the ligancy of a magnetically-active nickel(II) center can be reversibly switched between 4 and 5 as a result of the reversible folding and unfolding motion of a ligand-tipped electromechanical hinge based on 4,4'-bipyrinium units, best known as viologens.

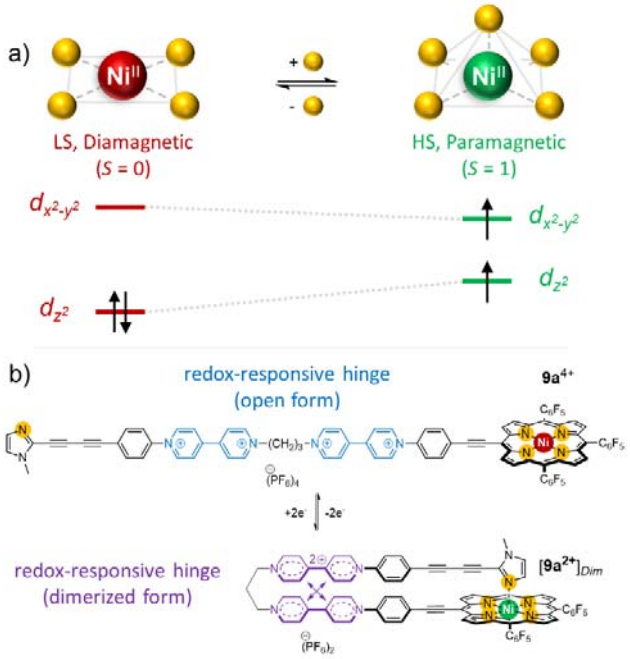

Figure 1. (a) Schematic representation of the spin-state switching by coordination/dissociation of an exogenous ligand to/from a Ni(II)-porphyrin. Ligands are represented by yellow spheres (b) Electron-triggered reversible folding/unfolding process in **9a**$^{4+}$ accompanied by coordination/dissociation of the endogenous ligand.

The redox-responsive Ni(II)-porphyrin complex **9a**$^{4+}$ that was designed to achieve a remote control over the ligancy of a nickel center is made out of three key functional elements: *i*) a

magnetically active center in the form of a square planar Ni(II)-porphyrin bearing three electron-withdrawing *meso*-substituents introduced to improve the affinity of the square planar low spin (LS) S= 0 Ni(II) center for axial coordination;[51] *ii*) an electromechanical hinge (actuator) incorporating two dicationic 4,4′-bipyridinium subunits ($\mathbf{V}^{2+}$) linked through a flexible propylene linker in such a way as to promote the formation of intramolecular π-dimers at the reduced state ($2\mathbf{V}^{+\bullet} \rightarrow [\mathbf{V_2}]^{2+}_{Dim}$)[52,53] and iii) an endogenously tethered imidazole ligand, selected for its high affinity for the Ni(II) center, introduced at the tip of the actuator through a sequence of ethynyl/phenyl units.[50]

We show in the present article that $\mathbf{9a}^{4+}$ adopts an elongated conformation in solution, imposed by repulsive electrostatic forces between the dicationic bipyridinium units, wherein the square planar nickel center lies in a diamagnetic low spin state ($S = 0$). We have then established that this compound undergoes an electron-triggered mechanical folding, driven by the dimerization between the electrogenerated bipyridinium cation radicals ($\mathbf{V}^{+\bullet}$),[50,54,5550,52,54–59] leading to a forced coordination of the imidazole ligand coming along with a change in the electronic configuration of the metal LS ($S = 0$) → HS ($S = 1$).[31,51]

RESULTS AND DISCUSSION

Syntheses. Both metalloporphyrin-viologen compounds studied in this work, $\mathbf{9a}^{4+}$ and $\mathbf{9b}^{4+}$, differ by the presence of either pentafluorophenyl (electron-withdrawing groups) or propyl (electron-donating groups) substituents at the *meso* positions of the porphyrin ring, respectively. Those substituents were introduced to change the ability of the nickel(II) center to accept axial ligands. $\mathbf{9a}^{4+}$ and $\mathbf{9b}^{4+}$ were synthesized in five steps (Scheme 1), starting from the corresponding diaroylated or dialkanoylated dipyrromethanes **1a**[60] or **1b**[50] building on strategies previously developed in our group.[50,54,61] Reduction of **1a-b** with sodium borohydride afforded the corresponding dicarbinols intermediates which were further condensed with the *β*-free 2,2'-dipyrrolylmethane[60] under inert conditions and then oxidized with DDQ to give the targeted A_3B-type *meso*-substituted porphyrins **2a-b** in 29% and 24% yield, respectively. Subsequent metalation of the inner porphyrin with Nickel(II) acetylacetonate[23] and regioselective α-bromination of the remaining *meso*-free position with *N*-bromosuccinimide[60] afforded **4a** in 72% yield over two steps, while a reverse bromination-metalation sequence furnished porphyrin **4b** in 81% yield over two steps. The key amine-substituted intermediates **5a-b** were then obtained in 70% and 49% yield, respectively, as the product of palladium- and copper-catalyzed Sonogashira cross-coupling reactions[62] between **4a-b** and 4-ethynylaniline. The targeted compounds $\mathbf{9a\text{-}b}^{4+}$ were ultimately obtained in 60% and 77% yield respectively, from a Zincke coupling[54,63] reaction involving the ethynylaniline substituted porphyrins **5a-b** and the previously described 2,4-dinitrophenyl activated bis-viologen precursor $\mathbf{8}^{4+}$ as reactants.[50] The porphyrin-monoviologen $\mathbf{7}^{2+}$, used as a reference compound in our investigations, was obtained similarly in 66% yield from the mono-activated precursor $\mathbf{6}^{2+}$.[54]

Characterization of the open forms. The structures of $\mathbf{9a}^{4+}$, $\mathbf{9b}^{4+}$ were confirmed by High Resolution Mass Spectrometry (HRMS) (Figures ESI 35-37) and spectroscopic measurements. The full ^{1}H NMR spectra of both compounds recorded in deuterated acetonitrile at 1 mM are shown in Figures ESI 20 & 26. All peaks were fully assigned with the help of 1D and 2D (COSY and ROESY) experiments (see ESI section). The signals attributed to the viologen/phenyl/alkyl subunits are found to resonate at similar frequencies in both compounds. As expected, only the porphyrin-based peaks show noticeable shifts which can be explained by the drastic difference between the electronic effects of the propyl and pentafluorophenyl substituents. This effect is most apparent for the more deshielded peak attributed to the β-proton H_a (Scheme 1) observed at 10.06 and 9.60 ppm in the spectra of $\mathbf{9a}^{4+}$ and $\mathbf{9b}^{4+}$, respectively. To a lesser extent, the imidazole protons (H_n and H_o) follow a similar trend, together with a significant broadening of the signals observed in $\mathbf{9a}^{4+}$ relative to $\mathbf{9b}^{4+}$, suggesting an interaction between the available nitrogen atom and the electron-deficient porphyrin Ni-complex in $\mathbf{9a}^{4+}$.

Scheme 1. Synthesis of $\mathbf{7}^{2+}$, $\mathbf{9a}^{4+}$ and $\mathbf{9b}^{4+}$.[a]

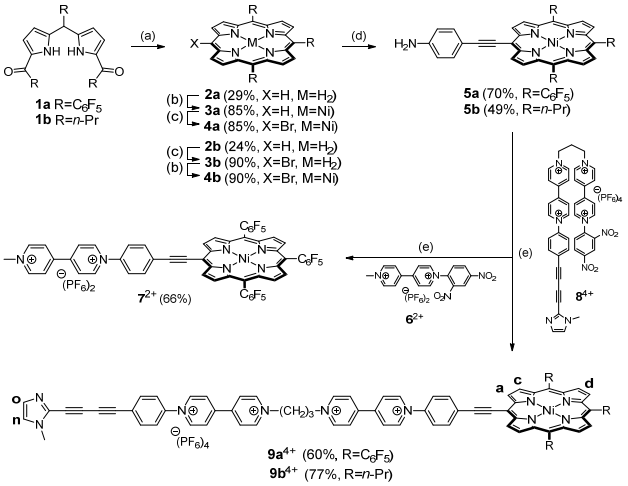

[a] Reaction conditions: (a) $NaBH_4$, MeOH:THF, 25 °C; then 2,2'-dipyrrolylmethane, $Yb(OTf)_3$ or TFA, CH_2Cl_2 or CH_3CN, 25 or 34 °C; then DDQ, 25 °C. (b) $Ni(acac)_2$, toluene, reflux. (c) NBS, pyridine, $CHCl_3$, 0 °C. (d) 4-Ethynylaniline, $PdCl_2(PPh_3)_2$, CuI, Et_3N, THF, 40 °C. (e) EtOH, CH_3CN, THF, 80 °C; then KPF_6, H_2O.[61] The lowercase letters shown on the final product will be used to discuss the attribution of the ^{1}H NMR signals to specific protons, *ie* Ha, Hb, H, Ho and Hn.

In line with these initial findings, the ability of the imidazole appended nickel(II) complexes to self-assemble in solution, through the formation of intermolecular coordination bonds between imidazole and nickel, was assessed from concentration dependent ^{1}H NMR measurements carried out in MeCN-d_3. Data collected with the propyl-substituted derivative $\mathbf{9b}^{4+}$ revealed that the signals assigned to the imidazole (H_o and H_n) do not shift significantly upon increasing the concentration from 0.1 to 10 mM (Figure ESI 31), which supports the conclusion that there is no intermolecular coordination occurring under these conditions. The large broadenings and high field shift conversely undergone on this concentration range by all the signals of the porphyrin (H_a, H_c and H_d) are therefore attributed to the formation of J-or H-type aggregates.[64] The absence of coordination bond between imidazole and nickel at 1 mM was then further demonstrated by Variable Temperature NMR (VT-NMR) measurements showing that the chemical shifts of both singlets assigned to imidazole do not change upon heating the sample from 278 to 313 K (Figure ESI 32).

Similar investigations were carried out on the C_6F_5-substituted analog $\mathbf{9a}^{4+}$, featuring an "activated" nickel center, more in-

clined to accept one or two additional ligands in axial position.[39,51,65] The spectra recorded over the 0.1-10 mM concentration range are shown in Figure 2. The two major differences with the data collected in the same condition with **9b**$^{4+}$ are the simultaneous downfield shift of the signals assigned to the imidazole and porphyrin units. These changes observed for concentrations greater than 1 mM have been attributed to the formation of short coordination oligomers in solution favored by the electron-withdrawing effect of the three C_6F_5 substituents. The large concentration required to trigger these changes is however consistent with a weak affinity of the imidazole for the metal center, a conclusion which was eventually confirmed by the quite weak binding constants estimated from NMR titration experiments involving 1-methylimidazole and **7**$^{2+}$ as reference ligand and metal complex, respectively (see ESI section for details). The ability of **9a**$^{4+}$ to self-assemble in solution was further investigated by diffusion-ordered spectroscopy (DOSY) measurements conducted at room temperature in MeCN-d_3 over a concentration range of 1-10 mM. Here again, the limited evolution of the calculated diffusion coefficient over this concentration range, decreasing from 614 (for the most diluted sample) to 505 $\mu m^2.s^{-1}$ (for the most concentrated sample) suggests the formation of small assemblies involving only a few monomers (n = 2 at 10 mM using a spherical model, see ESI section)

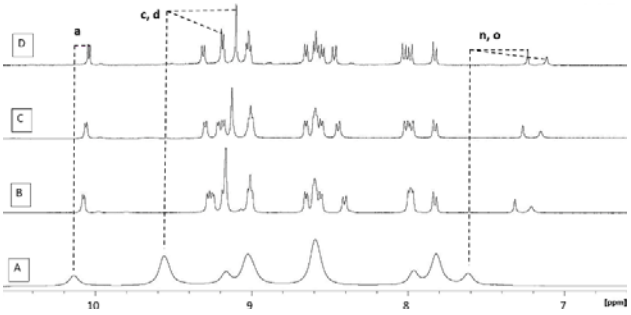

Figure 2. Partial ^{1}H NMR signature of **9a**$^{4+}$ in the aromatic region at (A) 10, (B) 2, (C) 1 and (D) 0.1 mM. The dotted lines represent the shifts of the porphyrin-(purple) and imidazole-based (green) peaks (298 K, MeCN-d_3, 400 MHz).

On the other hand, further analyses revealed a significant solvent-dependence of the absorption spectra of **9a**$^{4+}$, the most notable feature being a significant bathochromic-shift of the Soret band going from λ_{max} = 421 nm in the least coordinating solvent MeCN and 428 in DMF, up to 441 nm in the most coordinating solvent DMSO (Figure ESI 39A). The coordination ability of DMSO, and to a lesser extent of DMF, on the Ni-center was further demonstrated by ^{1}H NMR measurements with a broadening and downfield-shift of $\delta(H_a)$ from 10.06 ppm in MeCN-d_3 up to 10.98 ppm in DMF-d_7 and 26.4 ppm in DMSO-d_6 (Figure ESI 28). The particular behavior observed in DMSO, and most particularly the large low field shift of $\delta(H_a)$, was thus attributed to a partial conversion of the first coordination sphere of the Ni(II) center, from tetra-coordinated square planar to penta-coordinated square-based pyramid (with one molecule of DMSO in axial position) or hexacoordinated bipyramidal (with two molecules of DMSO in axial position), coming along with a partial change in the electronic configuration of the metal from low spin (S = 0) to high spin (S = 1).

These solvent effects proved to be far less marked with **9b**$^{4+}$, whose ^{1}H NMR spectra recorded in deuterated DMF or DMSO showed well-defined/sharp signals resonating between 0 and 10 ppm (Figure ESI 30). Opposite to the case of **9a**$^{4+}$, the most deshielded proton peaks were assigned to protons from the viologen units (H_b and H_e) rather than from the porphyrin (H_a). We also found that $\delta(H_a)$ undergoes only minor shift between MeCN-d_3 (9.60 ppm) and DMSO-d_6 (9.64 ppm). This solvent-independent behavior was also demonstrated by UV/vis experiments (Figure ESI 39B).

Characterization of the electron-triggered folding process. **9a**$^{4+}$, **9b**$^{4+}$ and the reference compound **7**$^{2+}$ were submitted to detailed electrochemical analyses carried out in DMF (+ 0.1 M electrolyte concentration), to ensure the solubility of all investigated species both at their oxidized and reduced states and to minimize the solvent effects discussed above affecting both the first coordination sphere and the magnetic properties of the metal center. Some key data collected with these compounds are given in Table 1.

As can be seen in Figure 3A, the cyclic voltammogram of **9a**$^{4+}$ exhibits one irreversible oxidation wave at E_p^{1a} = 0.78 V and four consecutive reversible reduction processes in the accessible potential range, i.e., above –2 V. The first two, higher-intensity waves observed at $E_{1/2}^{1c}$ = – 0.51 and $E_{1/2}^{2c}$ = – 1.05 V are attributed to the one-electron/viologen reductions yielding successively the dicationic bis-radical **9a**$^{2(+\bullet)}$ and the neutral quinonic **9a**^{0} species. These processes are followed by two waves of lower intensities at $E_{1/2}^{3c}$ = – 1.23 and $E_{1/2}^{4c}$ = – 1.77 V attributed to the consecutive one-electron reductions of the porphyrin ring affording a porphyrin anion radical and a porphyrin dianion (Figure ESI 49B).[66] This attribution is consistent with the relative intensities of the first two reduction waves which are twice as high as the two last ones and with the stoichiometry of the viologens (V) and porphyrin (P) units involved in **9a**$^{4+}$.

Table 1. Electrochemical data collected for 1 mM solutions (in viologen) of 9a^{4+}, 9b^{4+} and 7^{2+} in DMF + TBAP (0.1 M).[a]

Entry	Compound	E^{4c} $P^{\bullet-}/P^{2-}$	E^{3c} $P/P^{\bullet-}$	E^{2c} $V^{+\bullet}/V^0$	E^{1c} $V^{2+}/V^{+\bullet}$	E^{1a} $P/P^{+\bullet}$
1	**9a**$^{4+}$	-1.77 [b] (86) [d]	-1.23[b] (60)[d]	-1.05 [b] (40) [d]	-0.51[b] (48) [d]	0.78 [c]
2	**9b**$^{4+}$	-2.51[c]	-1.58[b] (63)[c]	-1.01[b] (40) [c]	-0.55 [b] (72) [c]	0.62 [c]
3	**7**$^{2+}$	-1.76 [b] (62) [d]	-1.23[b] (64)[d]	-0.96 [b] (62) [d]	-0.67 [b] (64) [d]	0.81[c]

[a] Glassy carbon WE, Φ = 3 mm, E *vs* E_{ref} [$Ag^+(10^{-2}$ M)/Ag]., ν = 0.1 V.s^{-1}. "P" and "V" stand for "porphyrin" and "viologen", respectively. [b] Half-wave potential value ($E_{1/2}$ in V); [c] peak potential value (E_{pa} or E_{pc} in V); [d] Peak to peak potential shift ($\Delta E_p = |E_{pa} - E_{pc}|$ in mV).

A similar signature was observed for the propyl-substituted analogs **9b**$^{4+}$. In agreement with the presence of electron donating *meso*-substituents, we found the porphyrin unit to be much easier to oxidize, and conversely much harder to reduce, in **9b**$^{4+}$ than in **9a**$^{4+}$ (Figures ESI 48 and 49A). This difference is best revealed by the 350 mV shift observed for the reversible porphyrin-based reduction wave ($P/P^{\bullet-}$) at E^{3c} (Table 1) between **9a**$^{4+}$ than in **9b**$^{4+}$. These substituents were conversely found to have less influence on the viologen-centered reduction processes which are observed at similar potential values in both compounds ($\Delta E^{1c} = \Delta E^{2c}$ = 40 mV).

The ability of $\mathbf{9a}^{4+}$ and $\mathbf{9b}^{4+}$ to dimerize following the one-electron reduction of the viologen units involved in the hinge was first revealed by comparing their electrochemical signatures to that of the monoviologen reference compound $\mathbf{7}^{2+}$ (dashed line in Figure 3 and Figure ESI 49C). The latter displays the expected four reversible waves attributed to the successive one electron reduction of the viologen and porphyrins units. A quick look at the CV curves of $\mathbf{7}^{2+}$ and $\mathbf{9a}^{4+}$ however reveals that the porphyrin ring is reduced at similar potential values in both compounds while the viologen units are much easier to reduce into the radical species, by about 160 mV, in $\mathbf{9a}^{4+}$ than in $\mathbf{7}^{2+}$. Another striking difference is the stability domain of the $\mathbf{V}^{+\bullet}$ state ($\Delta E = |\boldsymbol{E}^{\mathbf{2c}}_{\mathbf{1/2}} - \boldsymbol{E}^{\mathbf{1c}}_{\mathbf{1/2}}|$), which is found to be much larger for $\mathbf{9a}^{4+}$ (540 mV) or for $\mathbf{9b}^{4+}$ (460 mV) than for $\mathbf{7}^{2+}$ (290 mV). Both the ease of reduction of the viologens ($\mathbf{V}^{2+}$) and the stabilization of the cation radical state $\mathbf{V}^{+\bullet}$ are in fact well known phenomenological indicators revealing the existence of a π-dimerization reaction coupled to the first viologen-centered electron transfer (Scheme 2).[52,67] This intramolecular dimerization process only occurs in the bis-viologen derivatives $\mathbf{9a}^{4+}$ and $\mathbf{9b}^{4+}$ due to the presence of a flexible propyl linker capable of adopting either an *anti*-conformation in the open tetracationic forms ($\mathbf{9a}^{4+}$ and $\mathbf{9b}^{4+}$) or a *syn* conformation in the folded π-dimerized forms ($[\mathbf{9a}^{2+}]_{Dim}$ or $[\mathbf{9b}^{2+}]_{Dim}$, see Scheme 2). Then, the fact that the viologen units are more easily reduced in $\mathbf{9a}^{4+}$ ($\boldsymbol{E}^{\mathbf{1c}}_{\mathbf{1/2}}$ = 0.51 V) than is $\mathbf{9b}^{4+}$ ($\boldsymbol{E}^{\mathbf{1c}}_{\mathbf{1/2}}$ = 0.55 V) and that the stability domain of the viologen cation radical is larger for $\mathbf{9a}^{4+}$ (540 mV) than for $\mathbf{9b}^{4+}$ (460 mV) are compelling experimental proof demonstrating that the *meso* substituents of the porphyrin ring have an influence on the π-dimerization constant (K_{Dim} in Scheme 2), which provide the first evidence that the coordination of imidazole on the nickel center provides additional stability to the closed isomers $[\mathbf{9a}^{2+}]_{Dim}$ or $[\mathbf{9b}^{2+}]_{Dim}$. These initial hypotheses were eventually confirmed by spectroelectrochemical studies discussed in the following section.

The existence of a dimerization step coupled to electron transfer was further revealed by studying the influence of scan rate and of concentration on the shape and potential of the first viologen-centered reduction wave of $\mathbf{9a}^{4+}$ and $\mathbf{7}^{2+}$. We first established that the calculated peak-to-peak potential shift calculated for $\mathbf{7}^{2+}$ does not vary over the studied concentration and scan rate ranges (Figure 3B & C), indicating that the $\mathbf{7}^{2+}$ undergoes, on these time scales, a fully reversible (fast) reduction and that the electrogenerated species $\mathbf{7}^{+\bullet}$ do not form intermolecular dimers under these conditions. By subjecting $\mathbf{9a}^{4+}$ to similar studies, we found conversely that the $E_{1/2}$ and ΔE_p values calculated for the first reduction wave do not change over the concentration range 2.10^{-4}-2.10^{-3}, but that the scan rate applied at the electrode has a profound influence on the peak-to-peak potential difference ΔE_p (Figure 3B & C). This value goes from 140 mV measured at 4 V/s down to 40 mV measured at 10 mV/s, which is consistent with the existence of a chemical steps coupled to "fast" (Nernstian) electron transfers ($[E^{1c}]_1$ and $[E^{1c}]_2$ shown in Scheme 2). In other words, the electrochemical response is here controlled by diffusion and by the kinetics of the chemical steps involved in the process which are the intramolecular dimerization (K_{Dim} in Scheme 2) of the doubly reduced species $\mathbf{9a}^{2(+\bullet)} \leftrightarrow [\mathbf{9a}^{2+}]_{Dim}$ and the associated disproportionation reaction (K_{Disp} in Scheme 2) $\mathbf{9a}^{2(+\bullet)} \leftrightarrow \mathbf{9a}^{2(+\bullet)} + \mathbf{9a}^{4+}$, which is driven by the continuous consumption/stabilization of $\mathbf{9a}^{2+(+\bullet)}$ as a dimer. The 40 mV ΔE_p value calculated at low scan rates can thus be simply explained by the fact that the second electron transfer $[E^{1c}]_2$ can be achieved at a more positive potential than the first one $[E^{1c}]_1$.[67] In a first approximation based on the work of Richardson and Taube,[68] a K_{Disp} value of 1.44 was calculated from the experimental ΔE_p values measured at 10 mV/s by cyclic voltammetry. Then, a dimerization constant of about 5250 could be estimated from the CV data recorded with $\mathbf{9a}^{4+}$ and with the reference compound $\mathbf{7}^{2+}$ (see ESI section for details).

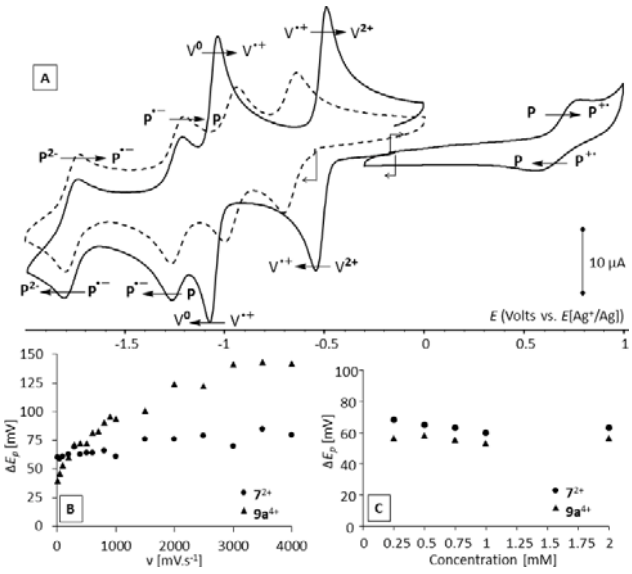

Figure 3. (A) Voltammetric curves of a DMF (0.1M TBAP) solution of $\mathbf{9a}^{4+}$ (solid lines) and $\mathbf{7}^{2+}$ (dashed line) (B) Peak to peak potential (ΔE_p) measured for $\mathbf{9a}^{4+}$ and $\mathbf{7}^{2+}$ at various scan rates (1 mM). (C) Peak to peak potential (ΔE_p) measured for $\mathbf{9a}^{4+}$ and $\mathbf{7}^{2+}$ at various concentrations (ν = 0.1 V s^{-1}, VC, Φ = 3 mm, E (volt) *vs* E_{ref}[Ag^+(10^{-2} M)/Ag].

Overall, these electrochemical data reveal that *i*) the kinetics of electron transfer centered on the viologen units (one electron per viologens) remains reversible (fast) in the investigated time scale (10mV to 4V/s); *ii*) the electrochemical response of $\mathbf{9a/b}^{4+}$ is driven by the kinetics of the coupled chemical steps; *iii*) there is no concentration effects and thus no intermolecular chemical association involved in solution in the concentration range (2.10^{-4}-2.10^{-3} M) neither with $\mathbf{9a}^{4+}$ nor with any of the in-situ electrochemically generated species $\mathbf{9a}^{2+(+\bullet)}$ or $\mathbf{9a}^{2(+\bullet)}$, and that *iv*) the doubly reduced species $\mathbf{9a}^{2(+\bullet)}$ is greatly stabilized by the intramolecular π-dimerization of the two viologen radicals involved in the hinge yielding the folded species $[\mathbf{9a}^{2+}]_{Dim}$.

The dimerization process yielding the intramolecular dimer $[\mathbf{9a}^{2+}]_{Dim}$ was then further characterized by spectroelectrochemistry (SEC) measurements carried out at platinum electrodes using either thin layer or large volume (~10 ml) SEC cells. The advancement of the electrochemical reactions and the stability of the *in-situ* generated reduced species (one e^-/viologens) at the electrolysis time scale (~hour) were systematically checked by rotating disk voltammetry measurements (see Figure ESI 50). Preliminary studies focused on the spectroscopic response of the reference compound $\mathbf{7}^{2+}$ to an exhaustive electrochemical reduction at E_{app} = –0.8 V. As expected, the one-electron reduction of the viologen led to the development of a broad signal at 670 nm (ε = 1.5 10^4 L·mol^{-1}·cm^{-1}) attributed to the electrogenerated free viologen radicals

coming along with a minor decrease (2 %) in the intensity of the Soret band (Figure ESI 52). Similar analyses where then carried out with $\mathbf{9a}^{4+}$ and $\mathbf{9b}^{4+}$ to gain insights into the folding process. As can be seen in Figure 4, the exhaustive electrolysis of a DMF (0.1 $TBAPF_6$) solution of $\mathbf{9a}^{4+}$ at E_{we}= –0.65 V led to major changes in the 300-1200 nm range. It includes a broad diagnostic band developing in the NIR region, at λ_{max} = 950 nm (ε = 6700 $L \cdot mol^{-1} \cdot cm^{-1}$), revealing the redox-triggered formation of the expected intramolecular π-dimers and whose energy provides direct information on the electronic-coupling between both bipyridinium radicals.[69]

Then, the ability of the terminal imidazole ligand to bind the nickel center, now brought nearby following the redox triggered mechanical folding, was demonstrated by the disappearance of the initial Soret band at 430 nm (ε = 1.1 10^5 $L \cdot mol^{-1} \cdot cm^{-1}$) at the expense of a new red-shifted band centered at 446 nm (ε = 1.3 10^5 $L \cdot mol^{-1} \cdot cm^{-1}$). This quite large 16 nm bathochromic shift of the Soret band proceeding through a well-defined isosbestic point at 436 nm is here fully consistent with a clean conversion of the open complex $\mathbf{9a}^{4+}$ into its folded isomer stabilized both by π-dimerization of the two viologen radicals and by the axial coordination of the imidazole on the nickel center ($[\mathbf{9a}^{2+}]_{Dim}$ in Scheme 2).

Scheme 2. A representative scheme of the stepwise viologen-centered reductions of $\mathbf{9a}^{2+}$ and the consecutive dimerization and disproportionation equilibria involved.

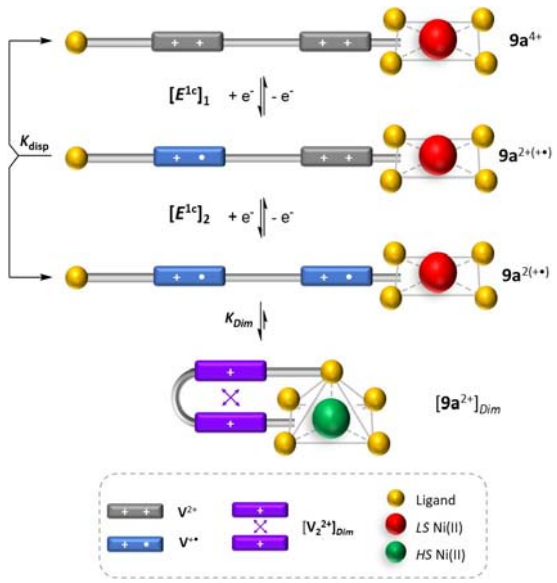

Further measurements carried out on the propyl substituted analog $\mathbf{9b}^{4+}$ led to similar changes in the NIR region with the development of a broad band attributed to the formation of the intramolecular dimer $[\mathbf{9b}^{2+}]_{Dim}$. On the other hand, as observed with $\mathbf{7}^{2+}$, the electrochemical reduction of the viologens proved to have very little influence on the Soret band which only features an intensity increase by about 10% without significant displacement of the absorption maximum (3 nm red shift). Comparison of these changes with those obtained under the same conditions with $\mathbf{9a}^{4+}$ thus led us to conclude that $\mathbf{9b}^{2(+\bullet)}$ undergoes an effective intramolecular dimerization yielding $[\mathbf{9b}^{2+}]_{Dim}$ but that this folding does not lead to the coordination of the imidazole to the electron-rich (relative to $\mathbf{9a}^{4+}$) nickel center.

In agreement with the proposed intramolecular process yielding $[\mathbf{9a}^{2+}]_{Dim}$, we also checked that the intensity of the dimer band at λ_{max} =950 nm and of the Soret band at 446 nm evolve linearly with concentration (ε_{950nm} = 6700 $L.mol^{-1}.cm^{-1}$; ε_{446nm} = 1.3 10^5 $L.mol^{-1}.cm^{-1}$, see Figure ESI 42). We next established that this species can be also easily produced using excess zinc powder as a chemical reducing agent and that the efficiency of the electron-triggered folding process can be assessed by ESR measurements. The spectra recorded after exhaustive (chemical) reduction of $\mathbf{9a}^{4+}$ and of $\mathbf{7}^{2+}$, used as a reference, are shown in Figure ESI 54. The intense and broad signal recorded after reduction of $\mathbf{7}^{2+}$ is consistent with the quantitative formation of free radicals unable to interact in these experimental conditions, while the residual signal observed from $\mathbf{9a}^{4+}$ attests to the strong displacement of the dimerization equilibrium (K_{Dim} in Scheme 2) in favor of the silent diamagnetic complex $[\mathbf{9a}^{2+}]_{Dim}$, the weak signal being attributed to the amount of non-associated bis radicals $\mathbf{9a}^{2(+\bullet)}$ (Scheme 2) that remains in solution.

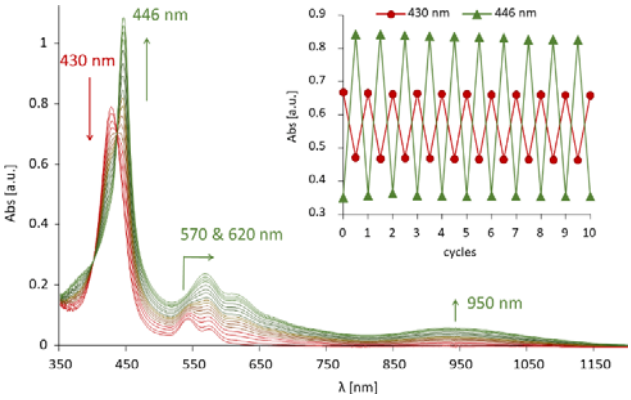

Figure 4. UV/vis spectra recorded during the exhaustive electrolysis (one electron per viologen) of $\mathbf{9a}^{4+}$ at 4.5 × 10^{-5} mol L^{-1} in DMF (0.1 M $TBAPF_6$) (working electrode: Pt, E_{app} = −0.65 V, 10 mL, l = 1 mm, t ≈ 1h). Increment: Switching cycles of $\mathbf{9a}^{4+}$ on thin-layer spectrolelectrochemistry during alternating reduction (E_{app}= −0.85 V) and re-oxidation (E_{app} = 0 V). The UV-vis absorptions at 430 (red; square planar Ni-porphyrin) and 446 nm (green; square pyramidal Ni-porphyrin) are plotted as a function of the number of switching cycles.

The reversibility of the redox-triggered folding motion ($\mathbf{9a}^{4+}$ ↔$[\mathbf{9a}^{2+}]_{Dim}$) was eventually checked by thin-layer spectroelectrochemistry by carrying out reduction/oxidation cycles. As can be seen in the inset of Figure 4, the system showed no fatigue after 10 consecutive reduction (E_{app} = –0.85 V) and back-oxidation (E_{app} = 0 V), as revealed by the complete recovery of the absorption at 430 and 446 nm throughout the process.

It has also been shown that both the dimerization and coordination of the appended 1-methylimidazole to Ni is favorable enough to occur even in presence of an excess of competing exogenous ligand like 1-methylimidazole (Figure ESI 53). This was revealed from the concomitant growth of the characteristic π-dimer band at 950 nm together with the 6 nm bathochromic shift of the Soret band (441 to 447 nm) which can be attributed to the ejection of one exogenous ligand initially bound to Nickel in the open form and to the coordination of the covalently-linked terminal imidazole brought right above the metal by the folding process.

These SEC data discussed above thus provide clear evidence supporting the conclusion that the electrochemical reduction of $\mathbf{9a}^{4+}$ (one electron/viologens) triggers a large amplitude folding motion allowing to force the axial coordination of the tethered 1-methylimidazole ligand on the nickel center. This process is fully reversible and comes along with a change in the coordination sphere of the metal center going from square planar to square pyramidal. This increase in coordination number is however only observed when the porphyrin ring is depleted by electron-withdrawing substituents (Figure ESI 51).

Magnetic properties. Further studies aimed at studying the change in magnetic properties associated to the electron-triggered metamorphic process. In agreement with the schematic drawing shown in Figure 1a, it was indeed expected that the folding motion and the resulting change in the coordination number of the Ni(II) center, going from tetracoordinated square planar in $\mathbf{9a}^{4+}$ to pentacoordinated square pyramidal in $[\mathbf{9a}^{2+}]_{Dim}$ could trigger a drastic change in the spin state of the metal from low spin (S = 0) to high spin (S = 1).[39,51,70] These assumptions were confirmed by NMR measurement carried out before and after reduction of $\mathbf{9a}^{4+}$ in MeCN-d_3. The diamagnetic LS state of this tetracationic species was first demonstrated by the ^{1}H NMR spectrum recorded at 1 mM (see Figure 2C), mainly through the observation of all the expected well-resolved signals within a fairly standard window (0-10 ppm). The influence of axial coordination on the magnetic state of the Ni(II) center was also initially checked by running the ^{1}H NMR of $\mathbf{9a}^{4+}$ in pyridine-d_5 (Figure ESI 29) or upon addition of 1-methylimidazole in excess to the reference compound $\mathbf{7}^{2+}$ (see titration curves displayed in Figure 5 and ESI section for details).

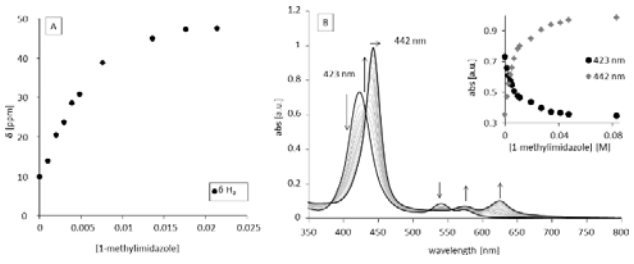

Figure 5. (A) Variation of δ_{Ha} *vs* the concentration in 1-methylimidazole for $\mathbf{7}^{2+}$ (1 mM MeCN-d_3, 400MHz, 298K). (B) UV/vis spectra recorded during the progressive addition of 1-methylimidazole to a solution of $\mathbf{7}^{2+}$ (MeCN, 5.92 10^{-5} M, l = 1 mm); Increment: variation of the absorption at λ_{max}= 423 & 442 nm *vs* concentration of 1-methylimidazole.

As an illustration of that behavior, we found that the gradual addition of 1-methylimidazole leads to large broadenings/shifts or even disappearance of the ^{1}H NMR signals, including a 43 ppm down field shift, from δ_i = 10 ppm to δ_f = 53 ppm (recorded after addition of 120 molar equivalents of 1-methylimidazole ligand), of the singlet attributed to one of the β-proton atoms H_a. Similar titrations followed by UV-visible absorbance spectroscopy showed that the binding of 1-methylimidazole results in the progressive decrease in the intensity of the initial Soret band at 423 nm at the expense of a new band at 442 nm reaching full development after addition of about 1600 molar equivalents of 1-methylimidazole ligand. Fitting the NMR data with a 2:1 (L:M) binding model,[39] based on the well-accepted idea that the coordination of one axial ligand (K_1) promotes the addition of a second (K_2) on the opposite face of the Ni-porphyrin, led us to estimate the association constants K_1 and K_2 to 110 M^{-1} and 90 M^{-1}, respectively. The slightly higher K_1 value can be correlated to the electron-deficiency of the porphyrin ring surrounded by three C_6F_5-and a viologen unit as EWGs.[39] These preliminary studies carried out with a reference compound $\mathbf{7}^{2+}$ thus revealed that imidazole has a fairly moderate affinity for the nickel center and that its addition leads to a strong downfield shifts of the ^{1}H NMR signals, reaching up to 53 ppm for the protons of the porphyrin, accompanied by a bathochromic 19 nm shift of the Soret band in MeCN, a behavior which is strongly reminiscent to that observed during the reduction of $\mathbf{9a}^{4+}$ in DMF (0.1M $TBAPF_6$) (Figure 4).

Then, our attention focused on the ^{1}H NMR signature of the folded species $[\mathbf{9a}^{2+}]_{Dim}$ produced by chemical or electrochemical reduction of the open form $\mathbf{9a}^{4+}$. The ^{1}H NMR spectrum recorded after chemical reduction (1e^-/viologen) of a 1 mM solution of $\mathbf{9a}^{4+}$ in deuterated acetonitrile (Figure 6 and Figures ESI 55 & 56) displays distinct features including 5 peaks observed between 40 and 50 ppm, one broad singlet at –2 ppm and several broad and unresolved signals still resonating in the 0-10 ppm window. Based on literature data reported for similar C_6F_5-substituted HS Ni porphyrins,[23,31] these four broad peaks observed above 43 ppm were attributed to the resonances of H_a, H_c and H_d in the HS Nickel complex $[\mathbf{9a}^{2+}]_{Dim}$.[71] The less intense broad singlet at 38.5 ppm integrating for 1 proton was then attributed to the imidazole proton H_o which ends up being in close proximity to the paramagnetic center in the folded isomer.

Using equation (1),[31] which gives the molar ratio of the HS paramagnetic complex $[\mathbf{9a}^{2+}]_{Dim}$ (n_{para}) as a function of the chemical shifts of $[\mathbf{9a}^{2+}]_{Dim}$ (δ) and $\mathbf{9a}^{4+}$ (δ_{dia} in MeCN-d_3 and δ_{para} in pyridine-d_5), we were able to calculate the switching efficiency at 80% and then the effective magnetic moment, including Pascal's diamagnetic correction, at μ_{eff} = 3.05 μ_B (See ESI section for details) at 293 K, following the Evans method, which is within the range expected for a divalent HS Ni complex (S = 1).[23,72,73]

$$n_{para} = \frac{\delta - \delta_{dia}}{\delta_{para} - \delta_{dia}} = \frac{47.9-10.1}{57.1-10.1} = 0.80 \qquad \text{Eq. (1)}$$

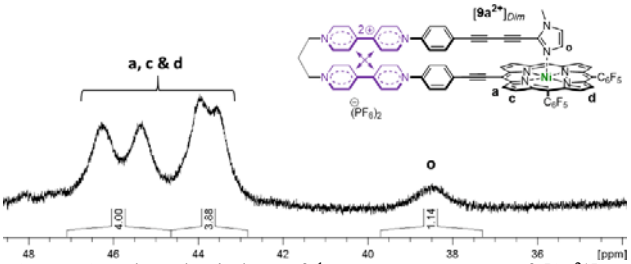

Figure 6. Selected window of ^{1}H NMR spectrum of $[\mathbf{9a}^{2+}]_{Dim}$ upon chemical reduction showing the downfield shifted proton peaks (1mM, MeCN-d_3, 293K).

Theoretical calculations. The folding process was further characterized by computational chemistry. DFT calculations were performed at the CAM-B3LYP/6-31+G(d,p)/SDD level of theory on the oxidized and reduced forms of the folded and unfolded isomers. As expected, we found that the folding of the fully-oxidized form $\mathbf{9a}^{4+}$ to be energetically disadvantaged,

by about +5.3 kcal.mol^{-1}, under the effect of repulsive electrostatic forces arising between the two viologen units. The folded isomer was conversely found to be strongly stabilized (-36.1 kcal.mol^{-1}, see Figure 7) at the reduced state (1e^{-}/viologen) by two complementary processes i) the overlap of SOMO centered on the viologen moieties yielding a sandwich-like π-dimer with an interplanar distance of about 3.2 Å and ii) by the formation of a 2.06 Å Ni-N coordination bond involving the terminal imidazole ligand.

TDDFT calculations performed at the same level of theory (CAM-B3LYP/6-311+G(d,p)/SDD) led to 50 states lying in good agreement with the experimental spectrum shown in Figure 4, in particular for the characteristic band centered at 960 nm (see Figure ESI 57 & 58).

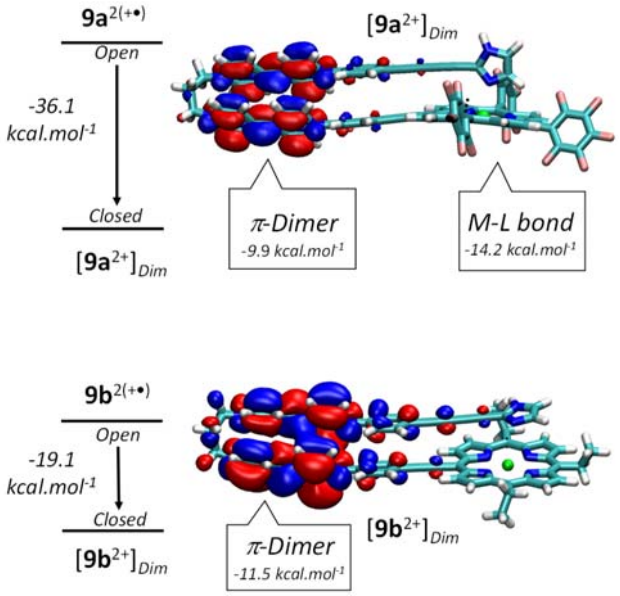

Figure 7. Schematic representation of the energy difference between the open **9a/b**$^{2(+•)}$ and closed isomers and [**9a/b**$^{2+}$]$_{Dim}$ and of the energy minimized π-dimers [**9a/b**$^{2+}$]$_{Dim}$.

In agreement with the experimental data discussed above, we found that a substitution of the -C_6F_5 groups by –C_3H_7 leads to the formation of a folded architecture featuring an unbound imidazole ligand lying flat with respect to the porphyrin plane (Figure 7). The absence of M-L bond in the folded isomer results in a significant drop in the stabilization energy down to -19.1 kcal.mol^{-1}. These major differences allow to conclude that both the π-dimerization of viologen cation radicals and the N-Ni coordination bond contribute by about 10 and 14 kcal.mol^{-1} to the total stabilization energy of [**9a**$^{2+}$]$_{Dim}$.

CONCLUSION

We have reported the synthesis and the magnetic properties of a redox-responsive tweezer-like molecule featuring a tethered imidazole ligand linked to a Ni(II) porphyrin through a flexible mechanical hinge capable of undergoing a large amplitude and fully reversible folding motion under the effect of electrical stimulations. On the ground of NMR, (spectro)electrochemical and magnetic studies supported by quantum calculations, we have shown that this well mastered and fully reversible molecular motion can be exploited to force the axial coordination of the appended imidazole ligand onto the square planar Ni(II) center, thereby triggering a change in its spin state from low spin (S = 0) to high-spin (S = 1). We believe that this first example of electron-triggered CISSS, involving large amplitude molecular motion triggered by simple reduction of viologen units, opens up new opportunities for the development of electronic and spintronic devices.

ASSOCIATED CONTENT

Supporting Information

The Supporting Information is available free of charge at https://pubs.acs.org/doi/10.1021/xxxxx.

Equipment and methods, experimental procedures and characterizations, electrochemical data, Evans measurements and computational details (PDF)

AUTHOR INFORMATION

Corresponding Authors

Christophe Bucher – *ENSL, CNRS, Laboratoire de Chimie UMR 5182, 46 allée d'Italie, 69342 Lyon, France;* orcid.org/0000-0003-1803-6733; Email: christophe.bucher@ens-lyon.fr

Floris Chevallier − *ENSL, CNRS, Laboratoire de Chimie UMR 5182, 46 allée d'Italie, 69342 Lyon, France;* orcid.org/0000-0002-7482-9351; Email: floris.chevallier@ens-lyon.fr

Authors

Shaymaa Al Shehimy − *Laboratoire de Chimie, ENS de Lyon, Univ. Lyon, CNRS UMR 5182, 69342 Lyon, France;* orcid.org/0000-0001-6486-0868

Orsola Baydoun − *Laboratoire de Chimie, ENS de Lyon, Univ. Lyon, CNRS UMR 5182, 69342 Lyon, France*

Sandrine Denis-Quanquin − *Laboratoire de Chimie, ENS de Lyon, Univ. Lyon, CNRS UMR 5182, 69342 Lyon, France;* orcid.org/0000-0002-6746-7831

Jean-Christophe Mulatier *Laboratoire de Chimie, ENS de Lyon, Univ. Lyon, CNRS UMR 5182, 69342 Lyon, France;* orcid.org/0000-0001-7949-2666

Lhoussain Khrouz − *Laboratoire de Chimie, ENS de Lyon, Univ. Lyon, CNRS UMR 5182, 69342 Lyon, France ;* orcid.org/0000-0001-7098-8534

Denis Frath − *Laboratoire de Chimie, ENS de Lyon, Univ. Lyon, CNRS UMR 5182, 69342 Lyon, France;* orcid.org/0000-0001-6888-9377

Élise Dumont − *Laboratoire de Chimie, ENS de Lyon, Univ. Lyon, CNRS UMR 5182, 69342 Lyon, France;* orcid.org/0000-0002-2359-111X

Muralee Murugesu − *Department of Chemistry and Biomolecular Sciences, University of Ottawa, Ottawa, Ontario, K1N 6N5, Canada;* orcid.org/0000-0002-5123-374X

Funding

This work was funded by the École Doctorale de Chimie de Lyon, the École Normale Supérieure de Lyon, the GDR CNRS 2067 Macrocycles Pyrroliques, the Région Auvergne-Rhône-Alpes (PAI 2019) and the IDEX 2020 International Joint Research Chairs (IDEX/INT/2020/19 OPE-2020-0088).

Notes

The authors declare no competing financial interest.

ACKNOWLEDGMENTS

We gratefully acknowledge Delphine Pitrat, Claire Bourmaud and Aurore Valex (ENS de Lyon) for their contributions to this study.

REFERENCES

(1) Sato, O.; Tao, J.; Zhang, Y.-Z. Control of Magnetic Properties through External Stimuli. *Angew Chem Int Ed* **2007**, *46*, 2152–2187.

(2) Khusniyarov, M. M. How to Switch Spin-Crossover Metal Complexes at Constant Room Temperature. *Chem Eur J* **2016**, *22*, 15178–15191.

(3) Doistau, B.; Benda, L.; Hasenknopf, B.; Marvaud, V.; Vives, G. Switching Magnetic Properties by a Mechanical Motion. *Magnetochemistry* **2018**, *4*, 5.

(4) Kumar, K. S.; Ruben, M. Sublimable Spin-Crossover Complexes: From Spin-State Switching to Molecular Devices. *Angew Chem Int Ed* **2021**, *60*, 7502–7521.

(5) Čavlović, D.; Juríček, M. Molecular Magnetic Switches. *Chimia* **2019**, *73*, 313–316.

(6) Yao, Z.-S.; Tang, Z.; Tao, J. Bistable Molecular Materials with Dynamic Structures. *Chem Commun* **2020**, *56*, 2071–2086.

(7) Baroncini, M.; Silvi, S.; Credi, A. Photo- and Redox-Driven Artificial Molecular Motors. *Chem. Rev.* **2020**, *120*, 200–268.

(8) Aguilà, D.; Prado, Y.; Koumousi, E. S.; Mathonière, C.; Clérac, R. Switchable Fe/Co Prussian Blue Networks and Molecular Analogues. *Chem. Soc. Rev.* **2015**, *45*, 203–224.

(9) Ekanayaka, T. K.; Hao, G.; Mosey, A.; Dale, A. S.; Jiang, X.; Yost, A. J.; Sapkota, K. R.; Wang, G. T.; Zhang, J.; N'Diaye, A. T.; Marshall, A.; Cheng, R.; Naeemi, A.; Xu, X.; Dowben, P. A. Nonvolatile Voltage Controlled Molecular Spin-State Switching for Memory Applications. *Magnetochemistry* **2021**, *7*, 37.

(10) Gütlich, P.; Gaspar, A. B.; Garcia, Y. Spin State Switching in Iron Coordination Compounds. *Beilstein J Org Chem* **2013**, *9*, 342–391.

(11) Larionov, S. V. Spin Transition in Iron(III) and Iron(II) Complexes. *Russ J Coord Chem* **2008**, *34*, 237–250.

(12) Gütlich, P.; Goodwin, H. A. Spin Crossover - An Overall Perspective. In *Spin Crossover in Transition Metal Compounds I*; Gütlich, P., Goodwin, H. A., Eds.; Top. Curr. Chem.; Springer: Berlin, Heidelberg, 2004; pp 1–47.

(13) Ekanayaka, T. K.; Maity, K. P.; Doudin, B.; Dowben, P. A. Dynamics of Spin Crossover Molecular Complexes. *Nanomaterials* **2022**, *12*, 1742.

(14) Wilson, B. H.; Ward, J. S.; Young, D. C.; Liu, J.-L.; Mathonière, C.; Clérac, R.; Kruger, P. E. Self-Assembly Synthesis of a [2]Catenane CoII Single-Molecule Magnet. *Angew. Chem. Int. Ed.* **2022**, *61*, e202113837.

(15) Handzlik, G.; Rzepka, K.; Pinkowicz, D. The Underexplored Field of Lanthanide Complexes with Helicene Ligands: Towards Chiral Lanthanide Single Molecule Magnets. *Magnetochemistry* **2021**, *7*, 138.

(16) Clérac, R.; Winpenny, R. E. P. Single-Molecule Magnets and Related Phenomena. In *50 Years of Structure and Bonding – The Anniversary Volume*; Mingos, D. M. P., Ed.; Structure and Bonding; Springer International Publishing: Cham, 2017; pp 35–48.

(17) Feltham, H. L. C.; Brooker, S. Review of Purely 4f and Mixed-Metal Nd-4f Single-Molecule Magnets Containing Only One Lanthanide Ion. *Coord. Chem. Rev.* **2014**, *276*, 1–33.

(18) Real, J. A.; Gaspar, A. B.; Muñoz, M. C. Thermal, Pressure and Light Switchable Spin-Crossover Materials. *Dalton Trans.* **2005**, 2062–2079.

(19) Tailleur, E.; Marchivie, M.; Daro, N.; Chastanet, G.; Guionneau, P. Thermal Spin-Crossover with a Large Hysteresis Spanning Room Temperature in a Mononuclear Complex. *Chem. Commun.* **2017**, *53*, 4763–4766.

(20) Lavrenova, L. G.; Shakirova, O. G. Spin Crossover and Thermochromism of Iron(II) Coordination Compounds with 1,2,4-Triazoles and Tris(Pyrazol-1-Yl)Methanes. *Eur. J. Inorg. Chem.* **2013**, *2013*, 670–682.

(21) Brooker, S. Spin Crossover with Thermal Hysteresis: Practicalities and Lessons Learnt. *Chem. Soc. Rev.* **2015**, *44*, 2880–2892.

(22) Collet, E.; Guionneau, P. Structural Analysis of Spin-Crossover Materials: From Molecules to Materials. *Comptes Rendus Chim.* **2018**, *21*, 1133–1151.

(23) Venkataramani, S.; Jana, U.; Dommaschk, M.; Sönnichsen, F. D.; Tuczek, F.; Herges, R. Magnetic Bistability of Molecules in Homogeneous Solution at Room Temperature. *Science* **2011**, *331*, 445–448.

(24) Thies, S.; Sell, H.; Schütt, C.; Bornholdt, C.; Näther, C.; Tuczek, F.; Herges, R. Light-Induced Spin Change by Photodissociable External Ligands: A New Principle for Magnetic Switching of Molecules. *J. Am. Chem. Soc.* **2011**, *133*, 16243–16250.

(25) Volarić, J.; Szymanski, W.; Simeth, N. A.; Feringa, B. L. Molecular Photoswitches in Aqueous Environments. *Chem. Soc. Rev.* **2021**, *50*, 12377–12449.

(26) Shimizu, D.; Ide, Y.; Ikeue, T.; Osuka, A. Coordination-Induced Spin-State Switching of an Aminyl-Radical-Bridged Nickel(II) Porphyrin Dimer between Doublet and Sextet States. *Angew. Chem. Int. Ed.* **2019**, *58*, 5023–5027.

(27) Nowak, R.; Prasetyanto, E. A.; Cola, L. D.; Bojer, B.; Siegel, R.; Senker, J.; Rössler, E.; Weber, B. Proton-Driven Coordination-Induced Spin State Switch (PD-CISSS) of Iron(II) Complexes. *Chem. Commun.* **2017**, *53*, 971–974.

(28) Shankar, S.; Peters, M.; Steinborn, K.; Krahwinkel, B.; Sönnichsen, F. D.; Grote, D.; Sander, W.; Lohmiller, T.; Rüdiger, O.; Herges, R. Light-Controlled Switching of the Spin State of Iron(III). *Nat Comm* **2018**, *9*, 4750.

(29) Fischer, K.; Krahmer, J.; Tuczek, F. Chemically and Light-Driven Coordination-Induced Spin State Switching (CISSS) of a Nonheme-Iron Complex. *Z. Für Naturforschung B* **2022**, *77*, 299–311.

(30) Kropp, H.; Scheurer, A.; Heinemann, F. W.; Bendix, J.; Meyer, K. Coordination-Induced Spin-State Change in Manganese(V) Complexes: The Electronic Structure of Manganese(V) Nitrides. *Inorg. Chem.* **2015**, *54*, 3562–3572.

(31) Dommaschk, M.; Schütt, C.; Venkataramani, S.; Jana, U.; Näther, C.; Sönnichsen, F. D.; Herges, R. Rational Design of a Room Temperature Molecular Spin Switch. The Light-Driven Coordination Induced Spin State Switch (LD-CISSS) Approach. *Dalton Trans* **2014**, *43*, 17395–17405.

(32) Dommaschk, M.; Peters, M.; Gutzeit, F.; Schütt, C.; Näther, C.; Sönnichsen, F. D.; Tiwari, S.; Riedel, C.; Boretius, S.; Herges, R. Photoswitchable Magnetic Resonance Imaging Contrast by Improved Light-Driven Coordination-Induced Spin State Switch. *J Am Chem Soc* **2015**, *137*, 7552–7555.

(33) Dommaschk, M.; Näther, C.; Herges, R. Synthesis of Functionalized Perfluorinated Porphyrins for Improved Spin Switching. *J Org Chem* **2015**, *80*, 8496–8500.

(34) Heitmann, G.; Feiler, C.; Herges, R. Spin State Switching in Solution with an Azoimidazole-Functionalized Nickel(II)-Porphyrin. *Eur J Org Chem* **2016**, 3817–3823.

(35) Heitmann, G.; Schütt, C.; Gröbner, J.; Huber, L.; Herges, R. Azoimidazole Functionalized Ni-Porphyrins for Molecular Spin Switching and Light Responsive MRI Contrast Agents. *Dalton Trans* **2016**, *45*, 11407–11412.

(36) Wellm, V.; Groebner, J.; Heitmann, G.; Sönnichsen, F. D.; Herges, R. Towards Photoswitchable Contrast Agents for Absolute 3D Temperature MR Imaging. *Angew Chem Int Ed* **2021**, *60*, 8220–8226.

(37) Griffith, J. S.; Orgel, L. E. Ligand-Field Theory. *Q. Rev. Chem. Soc.* **1957**, *11*, 381–393.

(38) Ludwig, J.; Gröbner, J.; Dommaschk, M.; Huber, L. M.; Peters, M. K.; Hövener, J.-B.; Herges, R. Ni(II)Porphyrins as PH Dependent Light-Driven Coordination-Induced Spin-

State Switches (LD-CISSS) in Aqueous Solution. *J. Porphyr. Phthalocyanines* **2020**, *24*, 480–488.

(39) Thies, S.; Bornholdt, C.; Köhler, F.; Sönnichsen, F. D.; Näther, C.; Tuczek, F.; Herges, R. Coordination-Induced Spin Crossover (CISCO) through Axial Bonding of Substituted Pyridines to Nickel–Porphyrins: σ-Donor versus π-Acceptor Effects. *Chem Eur J* **2010**, *16*, 10074–10083.

(40) Heitmann, G.; Schütt, C.; Gröbner, J.; Huber, L.; Herges, R. Azoimidazole Functionalized Ni-Porphyrins for Molecular Spin Switching and Light Responsive MRI Contrast Agents. *Dalton Trans.* **2016**, *45*, 11407–11412.

(41) Thies, S.; Sell, H.; Bornholdt, C.; Schütt, C.; Köhler, F.; Tuczek, F.; Herges, R. Light-Driven Coordination-Induced Spin-State Switching: Rational Design of Photodissociable Ligands. *Chem Eur J* **2012**, *18*, 16358–16368.

(42) Ballardini, R.; Balzani, V.; Credi, A.; Gandolfi, M. T.; Venturi, M. Artificial Molecular-Level Machines: Which Energy To Make Them Work? *Acc. Chem. Res.* **2001**, *34*, 445–455.

(43) Le Poul, N.; Colasson, B. Electrochemically and Chemically Induced Redox Processes in Molecular Machines. *ChemElectroChem* **2015**, *2*, 475–496.

(44) Ohtake, T.; Tanaka, H. Redox-Induced Actuation in Macromolecular and Self-Assembled Systems. *Polym. J.* **2016**, *48*, 25–37.

(45) Sato, O.; Iyoda, T.; Fujishima, A.; Hashimoto, K. Electrochemically Tunable Magnetic Phase Transition in a High-Tc Chromium Cyanide Thin Film. *Science* **1996**, *271*, 49–51.

(46) Ruiz-Molina, D.; Wurst, K.; Hendrickson, D. n.; Rovira, C.; Veciana, J. A Thermally and Electrochemically Switchable Molecular Array Based on a Manganese Schiff Base Complex. *Adv. Funct. Mater.* **2002**, *12*, 347–351.

(47) Tezgerevska, T.; Alley, K. G.; Boskovic, C. Valence Tautomerism in Metal Complexes: Stimulated and Reversible Intramolecular Electron Transfer between Metal Centers and Organic Ligands. *Coord. Chem. Rev.* **2014**, *268*, 23–40.

(48) Nguyen, M. T.; Jones, R. A.; Holliday, B. J. Incorporation of Spin-Crossover Cobalt(II) Complexes into Conducting Metallopolymers: Towards Redox-Controlled Spin Change. *Polymer* **2021**, *222*, 123658.

(49) Mathonière, C. Metal-to-Metal Electron Transfer: A Powerful Tool for the Design of Switchable Coordination Compounds. *Eur. J. Inorg. Chem.* **2018**, *2018*, 248–258.

(50) Kahlfuss, C.; Denis-Quanquin, S.; Calin, N.; Dumont, E.; Garavelli, M.; Royal, G.; Cobo, S.; Saint-Aman, E.; Bucher, C. Electron-Triggered Metamorphism in Porphyrin-Based Self-Assembled Coordination Polymers. *J Am Chem Soc* **2016**, *138*, 15234–15242.

(51) Amati, M.; Baerends, E. J.; Ricciardi, G.; Rosa, A. Origin of the Enhanced Binding Capability toward Axial Nitrogen Bases of Ni(II) Porphyrins Bearing Electron-Withdrawing Substituents: An Electronic Structure and Bond Energy Analysis. *Inorg. Chem.* **2020**, *59*, 11528–11541.

(52) Kahlfuss, C.; Saint-Aman, E.; Bucher, C. Redox-Controlled Intramolecular Motions Triggered by π-Dimerization and ΠmerizationProcesses. In *Organic Redox Systems: Synthesis, Properties, and Applications*; Nishinaga, T., Ed.; John Wiley and sons: New-York, 2016; pp 39–88.

(53) Hirayama, F. Intramolecular Excimer Formation. Diphenyl and Triphenyl Alkanes. *J Chem Phys* **1965**, *42*, 3163–3171.

(54) Iordache, A.; Retegan, M.; Thomas, F.; Royal, G.; Saint-Aman, E.; Bucher, C. Redox Responsive Porphyrin-Based Molecular Tweezers. *Chem Eur J* **2012**, *18*, 7648–7653.

(55) Kahlfuss, C.; Gibaud, T.; Denis-Quanquin, S.; Chowdhury, S.; Royal, G.; Chevallier, F.; Saint-Aman, E.; Bucher, C. Redox-Induced Molecular Metamorphism Promoting a Sol/Gel Phase Transition in a Viologen-Based Coordination Polymer. *Chem Eur J* **2018**, *24*, 13009–13019.

(56) Cai, K.; Zhang, L.; Astumian, R.; Stoddart, J. Radical-Pairing-Induced Molecular Assembly and Motion. *Nat. Rev. Chem.* **2021**, *5*.

(57) Jana, A.; Bähring, S.; Ishida, M.; Goeb, S.; Canevet, D.; Sallé, M.; Jeppesen, J. O.; Sessler, J. L. Functionalised Tetrathiafulvalene- (TTF-) Macrocycles: Recent Trends in Applied Supramolecular Chemistry. *Chem. Soc. Rev.* **2018**, *47*, 5614–5645.

(58) Wadhwa, K.; Nuryyeva, S.; Fahrenbach, A. C.; Elhabiri, M.; Platas-Iglesias, C.; Trabolsi, A. Intramolecular Redox-Induced Dimerization in a Viologen Dendrimer. *J. Mater. Chem. C* **2013**, *1*, 2302–2307.

(59) Correia, H. D.; Chowdhury, S.; Ramos, A. P.; Guy, L.; Demets, G. J.-F.; Bucher, C. Dynamic Supramolecular Polymers Built from Cucurbit[n]Urils and Viologens. *Polym. Int.* **2019**, *68*, 572–588.

(60) Frost, J. R.; Huber, S. M.; Breitenlechner, S.; Bannwarth, C.; Bach, T. Enantiotopos-Selective C-H Oxygenation Catalyzed by a Supramolecular Ruthenium Complex. *Angew Chem Int Ed* **2015**, *54*, 691–695.

(61) For Further Details See Supporting Information.

(62) Honjo, K.; Mori, H.; Osuka, A. An Ethyne-Bridged Porphyrin-Hexaphyrin-Porphyrin Triad That Undergoes a Thermal Transannular Cyclization. *Asian J. Org. Chem.* **2016**, *5*, 196–200.

(63) Cheng, W.-C.; Kurth, M. J. The Zincke Reaction. A Review. *Org. Prep. Proced. Int.* **2002**, *34*, 585–585.

(64) Kubát, P.; Lang, K.; Procházková, K.; Anzenbacher, P. Self-Aggregates of Cationic Meso-Tetratolylporphyrins in Aqueous Solutions. *Langmuir* **2003**, *19*, 422–428.

(65) Walker, F. A.; Hui, E.; Walker, J. M. Electronic Effects in Transition Metal Porphyrins. I. Reaction of Piperidine with a Series of Para- and Meta-Substituted Nickel(II) and Vanadium(IV) Tetraphenylporphyrins. *J. Am. Chem. Soc.* **1975**, *97*, 2390–2397.

(66) Al Shehimy, S.; Frath, D.; Dumont, E.; Chevallier, F.; Bucher, C. Synthesis and Electrochemistry of Free-Base Porphyrins Bearing Trifluoromethyl Meso-Substituents. *ChemElectroChem* **2022**, *9*, e202101604.

(67) Imabayashi, S.; Kitamura, N.; Tokuda, K.; Tazuke, S. Intramolecular Association of Viologen Dimer and Trimer Radical Cations. An Electrochemical and Spectroscopic Study. *Chem. Lett.* **1987**, *16*, 915–918.

(68) Richardson, D. E.; Taube, H. Determination of E20-E10 in Multistep Charge Transfer by Stationary-Electrode Pulse and Cyclic Voltammetry: Application to Binuclear Ruthenium Ammines. *Inorg. Chem.* **1981**, *20*, 1278–1285.

(69) Lu, J.-M.; Rosokha, S. V.; Kochi, J. K. Stable (Long-Bonded) Dimers via the Quantitative Self-Association of Different Cationic, Anionic, and Uncharged ð-Radicals: Structures, Energetics, and Optical Transitions. *J Am Chem Soc* **2003**, *125*, 12161–12171.

(70) Salaam, J.; Rivat, M.; Fogeron, T.; Hasserodt, J. Molecular Sensors Operating by a Spin-State Change in Solution: Application to Magnetic Resonance Imaging. *Anal. Sens.* **2021**, *1*, 11–29.

(71) Belle, C.; Bougault, C.; Averbuch, M.-T.; Durif, A.; Pierre, J.-L.; Latour, J.-M.; Le Pape, L. Paramagnetic NMR Investigations of High-Spin Nickel(II) Complexes. Controlled Synthesis, Structural, Electronic, and Magnetic Properties of Dinuclear vs Mononuclear Species. *J. Am. Chem. Soc.* **2001**, *123*, 8053–8066.

(72) P. Lever, A. B. The Magnetic Moments of Some Tetragonal Nickel Complexes. *Inorg. Chem.* **1965**, *4*, 763–764.

(73) Cotton, F. A.; Wilkinson, G. *Advanced Inorganic Chemistry*; Wiley: New-York, 1988.

Graphical Abstract, For Table of Contents Only

Ni-centered Coordination-Induced Spin-State Switching Triggered by Electrical Stimulations.

Shaymaa Al Shehimy, Orsola Baydoun, Sandrine Denis-Quanquin, Jean-Christophe Mulatier, Lhoussain Khrouz, Denis Frath, Élise Dumont, Muralee Murugesu, Floris Chevallier,* and Christophe Bucher*